Saenger, W. (1984) *Principles of Nucleic Acid Structure*, p 266, Springer-Verlag, New York.
Searle, M. S., Hall, J. G., Denny, W. A., & Wakelin, L. P. G. (1988) *Biochemistry 27*, 4340-4349.
Sinha, R. K., Talapatra, P., Mitra, A., & Mazumder, S. (1977) *Biochim. Biophys. Acta 474*, 199-209.
Wang, A. H.-J., Ughetto, G., Quigley, G. J., & Rich, A. (1987) *Biochemistry 26*, 1152-1163.
Waring, M. J. (1970) *J. Mol. Biol. 54*, 247-279.
Williams, L. D., Egli, M., Gao, Q., Bash, P., van der Marel, G. A., van Boom, J. H., Rich, A., & Frederick, C. A. (1990a) *Proc. Natl. Acad. Sci. U.S.A. 87*, 2225-2229.
Williams, L. D., Egli, M., Ughetto, G., van der Marel, G. A., van Boom, J. H., Quigley, G. J., Wang, A. H.-J., Rich, A., & Frederick, C. A. (1990b) *J. Mol. Biol. 215*, 313-320.
Zhang, X., & Patel, D. J. (1990) *Biochemistry 29*, 9451-9466.

Interaction of Berenil with the *Eco*RI Dodecamer d(CGCGAATTCGCG)$_2$ in Solution Studied by NMR†

Andrew N. Lane,*,‡ Terence C. Jenkins,*,§ Tom Brown,‖ and Stephen Neidle§

Laboratory of Molecular Structure, National Institute for Medical Research, The Ridgeway, Mill Hill, London NW7 1AA, U.K., Cancer Research Campaign Biomolecular Structure Unit, Institute of Cancer Research, Sutton, Surrey SM2 5NG, U.K., and Department of Chemistry, University of Edinburgh, Edinburgh EH9 3JJ, U.K.

Received July 10, 1990; Revised Manuscript Received September 11, 1990

ABSTRACT: The conformation of the *Eco*RI dodecamer d(CGCGAATTCGCG)$_2$ has been examined in solution by ^{1}H and ^{31}P NMR. Spin–spin coupling constants and nuclear Overhauser (NOE) enhancement spectroscopy show that all deoxyriboses lie in the south domain, with a small admixture of the north conformation (0–20%). The time dependence of the nuclear Overhauser enhancements also reveals a relatively uniform conformation at the glycosidic bonds (average angle, $\chi = -114°$). The average helical twist is 36.5° (9.8 base pairs per turn). Tilt angles are small (in the range 0 to −10°), and roll angles are poorly determined. Unlike single-crystal X-ray studies of the same sequence, there is no evidence for asymmetry in the structure. Both the NOE intensities and ^{31}P relaxation data imply conformational anomalies at the C3–G4/C9–G10 and the A5–A6/T7–T8 steps. Berenil binds in 1:1 stoichiometry to the dodecamer with high affinity (K_d = 1 μM at 298 K) and causes substantial changes in chemical shifts of the sugar protons of nucleotides Ado 5–Cyt 9 and of the H2 resonances of the two Ado residues. No significant asymmetry appears to be induced in the DNA conformation on binding, and there is no evidence for intercalation, although the binding site is not centrosymmetric. NOEs are observed between the aromatic protons of berenil and the H1′ of both Thy 7 and Thy 8, as well as to Ado 5 and Ado 6 H2. These results firmly establish that berenil binds via the minor groove and closely approaches the nucleotides Ado 6, Thy 7, and Thy 8. On the basis of quantitative NOE spectroscopy and measurements of spin–spin coupling constants, changes in the conformations of the nucleotides are found to be small. Using the observed NOEs between the ligand and the DNA together with the derived glycosidic torsion angles, we have built models that satisfy all of the available solution data. The berenil molecule binds at the 5′-AAT (≡5′-ATT on the complementary strand) site such that (i) favorable hydrogen bonds are formed between the charged amidinium groups and the N3 atoms of Ado 6 and Ado 18 and (ii) the ligand is closely isohelical with the floor of the minor groove.

NMR has been shown to be an excellent method for studying the interactions of ligands such as drugs with DNA fragments (Gao & Patel, 1989). Numerous investigations have determined the mode of interaction of intercalators and groove binding agents with DNA and the conformational consequences of binding.

Berenil [1,3-bis(4′-amidinophenyl)triazene, diminazene, structure I] is a DNA minor groove binding compound with

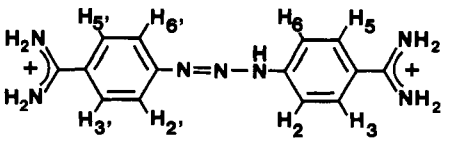

I

mild cytotoxic and antiviral properties (De Clercq & Dann, 1980) that is used extensively for the treatment of bovine trypanosomiasis. The compound shows preferential affinity for AT-rich tracts of DNA (Zimmer & Wähnert, 1986), and binding to double-stranded DNA has long been implicated in these biological effects. The interaction of berenil with DNA has been confirmed by DNase I and hydroxyl radical footprinting studies with a *Tyr* T fragment (Portugal & Waring, 1987; Laughton et al., 1990), which have revealed that the

† This work was supported by the Cancer Research Campaign, the Medical Research Council, and the Science and Engineering Research Council of the U.K.
* To whom correspondence (either author) should be addressed.
‡ National Institute for Medical Research.
§ Institute of Cancer Research.
‖ University of Edinburgh.

0006-2960/91/0430-1372$02.50/0

agent binds to both alternating AT and oligo(A) regions containing at least three contiguous AT base pairs.

Molecular modeling studies suggest that the "isohelical" concave surface of berenil is accommodated by the minor groove of DNA and that the ligand forms favorable directed hydrogen bonds with the bases (Gresh & Pullman, 1984; Pearl et al., 1987; Gago et al., 1989; Brown et al., 1990; Laughton et al., 1990). The crystal structure of the berenil–d-$(CGCGAATTCGCG)_2$ complex has recently shown (Brown et al., 1990) that the agent binds to the 5′-AAT (≡5′-ATT) sequence in the major groove of a B-form DNA structure, with hydrogen bonds from the amidinium groups to N3 of an adenine at each end of the binding site. The interaction is, however, indirect at the 5′-end, as a bridging water molecule mediates between the DNA and the bound ligand.

It is hoped that by understanding the processes involved in the recognition of defined DNA base sequences, rational modifications of the basic molecular structure can be engineered to modulate both binding affinity and site selectivity for therapeutic gain.

In this article we report a study of the interaction of berenil with the Dickerson dodecamer $d(CGCGAATTCGCG)_2$ using a combination of ^1H and ^{31}P NMR to determine the mode of binding in solution and the effects of the interaction on the conformation and dynamics of the DNA fragment. This sequence has been extensively studied by X-ray crystallography (Dickerson & Drew, 1981; Fratini et al., 1982). The structure has been determined under four different conditions, resulting in significant differences in both local conformation and global bending (Fratini et al., 1982). The molecule has also been the subject of numerous NMR investigations. Recently, Reid and co-workers (Nerdal et al., 1989) have reported a detailed solution structure of the dodecamer based on distance geometry and refinement by "back calculation" of the NOE[1] intensities. We prefer to use the calculation of the NOE intensities to drive the structure refinement directly in torsion space, which allows the effects of conformational averaging to be more easily modeled than distance geometry (Lane, 1990). We have therefore undertaken a detailed analysis of the solution conformation of the dodecamer using NMR so that the appropriate comparison with the complex formed with berenil can be made.

Materials and Methods

Materials

The *Eco*RI dodecanucleotide was synthesized on an Applied Biosystems synthesizer using phosphoramidite chemistry and purified by HPLC on a reverse-phase C8 column. The DNA was lyophilized and dissolved in 0.5 mL of 20 mM sodium phosphate, 100 mM KCl, and 0.1 mM EDTA in D_2O, pD* 7.0, containing 0.1 mM 4,4-dimethylsilapentane-1-sulfonate for chemical shift referencing. The concentration was 1.6 mM in strands.

Berenil (structure I) was synthesized via (i) diazotization of 4-aminobenzonitrile to 1,3-bis(4-cyanophenyl)triazene in 72% yield, (ii) conversion to the bis(amidine) in 61% yield by using the general procedure of Baker and Erickson (1967), and (iii) ion-exchange chromatography on Dowex-50W. The free base, which was homogeneous by HPLC, was converted to the *N*-acetylglycinate salt (93%) by using the method of Brodersen et al. (1958) and finally twice recrystallized from aqueous methanol to give yellow prisms, mp 482–483 K dec (lit. 475 K; Brodersen et al., 1958). The nonexchangeable proton resonances of berenil were assigned by NOE spectroscopy in dimethyl-d_6 sulfoxide at 298 K. The broad resonance at 10.9 ppm (which is the NH_2 resonance broadened by exchange with residual water) was irradiated for 0.5 and 2 s. A positive NOE was observed to the resonance at 8.1 ppm and a negative NOE to the resonance at 8.0 ppm. This result shows that the downfield resonance belongs to H3/H5 and the upfield resonance to H2/H6 (see structure I).

The complex of DNA with berenil was formed by mixing the ligand (2 mM) with the DNA (0.8 mM duplex) in 100 mM KCl and 2.5 mM sodium phosphate, pH 7.0, and then passing the mixture through a small column of Sephadex G-10 equilibrated in the same buffer system to remove excess ligand. Fractions, 0.5 mL, were collected, and those containing both berenil and DNA were pooled and lyophilized in the dark. The resulting dry powder was dissolved in 0.7 mL of 99.8% D_2O containing 0.1 mM 4,4-dimethylsilapentane-1-sulfonate, relyophilized, and finally dissolved in 0.5 mL of 99.98% D_2O for NMR analysis.

Methods

NMR Spectroscopy. ^1H NMR experiments were recorded at 400 or 500 MHz with a spectral width of 5 kHz. For one-dimensional experiments, 16 384 data points were collected with a relaxation delay time of 2.4 s (recycle time = 4.04 s). Truncated NOE experiments were done according to the method of Wagner and Wüthrich (1979). Spectra in ^1H_2O were acquired by using the $1\bar{3}3\bar{1}$ observation pulse (Hore, 1983). Correlation times of the cytosine H6–H5 vectors were determined from NOE time courses as previously described (Lane et al., 1986; Lane, 1989). NOESY spectra were recorded on the free DNA at different mixing times (50, 100, 150, and 200 ms) in the phase-sensitive mode by using the time-proportional phase increment scheme (Marion & Wüthrich, 1983); 2048 complex points were sampled in F2 and 512 in F1. The data matrices were zero-filled to 4096 points in both dimensions prior to Fourier transformation (digital resolution = 1.66 Hz/point). The free induction decays were apodized by using a 90°-shifted sine-squared bell in both. HOHAHA[1] spectra (Bax & Davis, 1985) were recorded similarly, with 4096 complex points zero-filled to 8192 points in F2 and 768 in F1, zero-filled to 1024 points, for a digital resolution of 1.22 Hz/point in F2. The isotropic mixing scheme was a MLEV-17 with 1.5-ms trim pulses at each end of the mixing period, which was 40 ms. The phase-sensitive double-quantum-filtered COSY[1] spectrum was also recorded with 4096 points in F2 and 768 points in F1, zero-filled in the same way. Both scalar correlated data sets were apodized by using 60°-shifted sine-squared bells in both dimensions. Sine-modulated data with the receiver phase set to 90° with respect to the transmitter, with optimization of the delay prior to the start of data acquisition, were collected in all two-dimensional experiments to eliminate t_1 ridges and produce a flat base plane (T. A. Frenkiel and C. J. Bauer, unpublished results). NOESY spectra of the complex were recorded at 50 and 150 ms.

NOESY cross-peak volumes were determined by multiplying together the line widths of cross sections parallel to F1 and F2 and the average peak height in the two cross sections (Chary et al., 1988). These were then normalized to the volume of a single proton for a zero mixing time. This was determined by taking the volume of an isolated diagonal peak at mixing time t_m and multiplying by $\exp(R_1 t_m)$, where R_1 is the selective spin–lattice relaxation rate constant independently

[1] Abbreviations: NOE, nuclear Overhauser enhancement; HOHAHA, homonuclear Hartmann–Hahn spectroscopy; CD, circular dichroism; COSY, correlated spectroscopy; CSA, chemical shift anisotropy.

determined from the initial slope of the recovery of a rapidly saturated spin using the sequence 90–t_1–90–acquire, where t_1 is the variable delay (Mirau, 1988). The volume used for normalization at mixing time was the average over all resolved base protons not including the Ado H2 resonances, which are partially saturated under the conditions of the NOESY experiments.

^{31}P NMR spectra were recorded at 81 MHz by using a 5-mm phosphorus probe and at 202.4 MHz by using a broad-band 5-mm probe. For measurements of R_2 the FRESCO modification of the Hahn spin–echo sequence was used (Forster, 1989), with a recycle time of 3 s. Protons were decoupled by using Waltz 16. Typically 10 relaxation delays were used, and the data were analyzed by nonlinear regression to the equation

$$M(t) = M^0 \exp(-R_2 t) \quad (1)$$

R_1 values were obtained by using FIRFT (Gupta et al., 1980) with 10 relaxation delays and a recycle time of 5 s. The recovery curves were analyzed by nonlinear regression to the equation

$$M(t) = a + b \exp(-R_1 t) \quad (2)$$

$\{^1H\}^{31}P$ NOEs were measured by broad-band irradiation of the protons for 10 s, with proton decoupling during the acquisition time (1.6 s). The NOEs were determined from difference spectra with and without irradiation during the relaxation delays.

Optical Spectroscopy. Ultraviolet difference spectra were recorded by using tandem cuvettes (d = 0.44 cm) on a Pye Unicam SP8-100 spectrophotometer with 2 μM duplex and 40 μM berenil in 5 mM sodium phosphate and 50 mM KCl, pH 7.0 at 298 K. CD[1] spectra were recorded in 1-cm path length cuvettes by using a Jasco Model J-600 spectropolarimeter. The duplex was titrated by addition of small aliquots of buffered berenil solution and recording the dichroism changes from 500 to 240 nm. Concentrations were determined from absorbances by using extinction coefficients of 23.1 mM^{-1} cm^{-1} at 380 nm for berenil and 3.83 mM^{-1} cm^{-1} at 258 nm for the dodecamer duplex.

NMR Data Analysis. Sugar puckers were determined from coupling constants as described by Rinkel and Altona (1987) and from NOE time courses by using NUCFIT (Lane, 1990). Other conformational parameters were determined by using both one- and two-dimensional NOE time courses, as described previously (Lane, 1990). Cross-relaxation rate constants for ligand–DNA interactions were determined by nonlinear regression by multispin analysis of NOE time courses as described previously (Lane & Forster, 1989). All fitting of primary data was carried out on Apple Macintosh computers.

Because the NMR data are local and directly define only the relationship between one base pair and its nearest neighbors, we have employed local helix axes as defined by Dieckmann et al. (1989). In this case, a positive roll is defined as a rotation of the 3′ base pair about its long axis to open the minor groove, a positive tilt opens the 3′ base pair in the minor groove, and a positive shift moves the 3′ base pair toward the minor groove.

Molecular Modeling and Energy Minimization. The initial coordinates of the d(CGCGAATTCGCG)$_2$ dodecamer were those of idealized canonical B-DNA (Arnott et al., 1983) and were prepared by using the program GENHELIX. Cartesian coordinates for berenil were derived from analysis of the crystal structures of berenil itself (Pearl et al., 1987) and structurally similar 1,3-diaryltriazenes (Walton et al., 1990). The molecule was asymmetric about the central nitrogen atom of the triazene linkage. Partial atomic charges for berenil were calculated from the semiempirical MNDO wavefunction, using the AMPAC (QCPE) program.

Interactive molecular modeling was performed by using the GEMINI 1.02 graphics program (Hampden Data Services Ltd., Abingdon, UK) with all visualizations on a Silicon Graphics Iris 4D-20G workstation. All calculations were carried out on an Alliant FX40/3 computer.

Models of the DNA–berenil complex were built initially by docking the ligand at a symmetric location within the minor groove such that no particular site was favored. The energy was minimized at the all-atom level by using X-PLOR (Brünger, 1988) together with the NMR-derived interproton distance data and dihedral constraints from glycosidic torsion angles. Additional parameters required for berenil were obtained by interpolation and from crystallographic data. The X-PLOR program, derived originally from CHARMm (Brooks et al., 1983), was adapted (Jiang and Hubbard, University of York, U.K., 1989) for use with the Alliant FX40 array processor.

The protocol employed for structure refinement is that recommended by Brünger (1990), using, stepwise, (i) 100 steps of conjugate-gradient minimization using only dihedral constraints, (ii) NOE-restrained and glycosidic torsion angle-constrained molecular dynamics with heating to 300 K followed by 5.0-ps dynamics at constant temperature (Nilsson et al., 1986; Nilsson & Karplus, 1986), and finally (iii) 400 steps of conjugate-gradient minimization. Typically, each minimization required 14100 cpu s on the Alliant FX40/3. Solvent and counterions were not explicitly included; instead their effects were simulated through the use of a distance-dependent dielectric constant with $\epsilon = 4r_{ij}$ for conjugate-gradient minimizations and $\epsilon = r_{ij}$ for the dynamics calculations. This formalism is well established in the arena of protein modeling and has recently been tested in a model nucleic acid system (Orozco et al., 1990). Further, no attempt was made to reduce the nett charge on the phosphate group (Tidor et al., 1983; Gronenborn & Clore, 1989). The hydrogen-bonded interactions were switched on for heavy-atom donor to acceptor distances between 0.55 and 0.65 nm, and terms up to 0.75 nm were included. Nonbonded energy terms were included up to 0.75 nm, with switching between 0.6 and 0.65 nm, and a factor of 0.4 was used to damp 1,4 electrostatic interactions. Explicit distance restraints corresponding to the Watson–Crick base-pairing geometry were not included.

Results and Discussion

Solution Conformation of d(CGCGAATTCGCG)$_2$. The conformation of the *Eco*RI recognition site has been examined in detail in the crystal state under four different conditions by Dickerson and co-workers (Fratini et al., 1982). Apart from the sequence dependence of the local conformation, one of the remarkable features of these structures is that three of them are bent, whereas one, in which Cyt 9 is brominated, is straight. The degree of bending appears to depend on temperature and crystallization conditions and is also associated with significant differences in many of the conformational parameters of the nucleotide units. These effects of crystal packing forces on conformation suggest that the dodecamer might be flexible in solution.

NMR data have indicated that the dodecamer is symmetric in solution (Patel et al., 1982, 1983; Hare et al., 1983; Nerdal et al., 1989). Further, although the crystal structures all have unique values for the backbone angle δ, which varies from 73° to 155° along the sequence, solution studies in general indicate a mixture of pucker states (Rinkel et al., 1987). Bax and Lerner (1988) have determined the coupling constants for the

Table I: Proton Assignments of the *Eco*RI Dodecamer at 303 K[a]

base	H8/6	Me/H5, H2	H1′	H2′	H2″	H3′	H4′	NH
			Free DNA					
Cyt 1	7.62	5.91	5.77	1.95	2.39	4.70	4.05	
Gua 2	7.94		5.88	2.63	2.71	4.96	4.33	13.19
Cyt 3	7.25	5.36	5.60	1.83	2.25	4.79	4.12	12.89
Gua 4	7.83		5.44	2.65	2.74	4.98	4.29	12.69
Ado 5	8.09	7.22	5.98	2.67	2.90	5.04	4.43	13.78
Ado 6	8.09	7.60	6.16	2.55	2.92	5.00	4.45	13.63
Thy 7	7.10	1.27	5.91	1.98	2.55	4.81	4.19	13.63
Thy 8	7.36	1.53	6.11	2.17	2.53	4.89	4.23	13.78
Cyt 9	7.46	5.61	5.66	2.06	2.40	4.87	4.14	12.69
Gua 10	7.89		5.85	2.62	2.69	4.98	4.36	12.89
Cyt 11	7.32	5.42	5.75	1.88	2.32	4.80	4.12	13.19
Gua 12	7.93		6.16	2.63	2.38	4.66	4.15	
			DNA–Berenil Complex					
Cyt 1	7.55	5.80	5.70	1.88	2.35	4.66	4.09	
Gua 2	7.89		5.83	2.61	2.68	4.94	4.32	12.97
Cyt 3	7.22	5.33	5.58	1.86	2.24	4.77	4.10	12.86
Gua 4	7.82		5.47	2.69	2.75	4.97	4.29	12.67
Ado 5	8.09	7.36	5.98	2.67	2.91	5.04	4.43	13.77
Ado 6	8.06	8.07	6.06	2.48	2.75	4.94	4.21	13.77
Thy 7	6.84	1.21	5.46	1.70	2.18	4.57	3.95	13.77
Thy 8	7.06	1.42	5.22	1.83	2.24	4.63	3.88	13.77
Cyt 9	7.25	5.52	5.48	1.87	2.25	4.78	4.17	12.67
Gua 10	7.85		5.80	2.60	2.64	4.96	4.35	12.86
Cyt 11	7.29	5.40	5.74	1.87	2.28	4.78	4.13	12.97
Gua 12	7.86		6.06	2.58	2.32	4.63	4.10	

[a] The protons were assigned by using NOESY, HOHAHA, and one-dimensional NOEs in H_2O as described in the text. Chemical shifts (δ, ppm) are referenced to internal DSS.

dodecamer and have shown that there is considerable variation of the fraction of the south state along the sequence. Therefore, to examine the effects of berenil on the conformation of the dodecamer, we have first characterized its conformation in the free state.

The ^{1}H NMR assignments have been reported by Hare et al. (1983), which we have confirmed by using a combination of NOESY, double-quantum-filtered COSY, and HOHAHA (data not shown). Only minor differences in chemical shifts are noted, which could be attributed to the slightly different solution conditions. The proton chemical shifts for the conditions of our experiments are given in Table I.

Temperature Dependence. The chemical shifts of the base protons all show a linear dependence on temperature in the range 278–313 K, with H8 resonances changing with a common slope and H2 resonances having opposite sign, as is commonly observed (Lefèvre et al., 1987; Lane, 1989). The line widths of resolved, single-base resonances all decrease monotonically with increasing temperature, with activation energies of 16–20 kJ mol^{-1}. There is no evidence for temperature-induced changes of conformation, even in the sequence GAAT, which is superficially similar to the conformationally flexible sequences TAAC and TAAT (Lefèvre et al., 1988; Lane, 1989).

Coupling Constants. As Altona and co-workers have shown (Rinkel & Altona, 1987; Rinkel et al., 1987), coupling constants in the deoxyriboses can be used to determine sugar pucker states and the equilibrium between the north (near C3′ endo) and south (near C2′ endo) states. Several H1′ resonances are resolved in one-dimensional spectra (cf. Figure 1), which demonstrate significant differences in coupling to H2′ and H2″, indicating the presence of different pucker states. To improve resolution and obtain information on the H2′/H2″ region, we ran double-quantum-filtered COSY and HOHAHA experiments under conditions of high digital resolution (approximately 1.2 Hz/point in F2). From these experiments, it is possible to determine sums of coupling constants, $\sum_{1'}$, $\sum_{2'}$, and $\sum_{2''}$, to a precision of about ±1 Hz, which is sufficient to place limits on the fraction of the south state (f_s) and the pseudorotation angle of the south state, P_s, with an error of around ±20°. The coupling constant data are given in Table II. Many of the sugars have significant fractions of the north conformer, which may account for differences in the pseudorotation phase angles compared with those derived from X-ray analyses of the crystal state. The coupling constants and derived sugar parameters are very similar to those determined by Bax and Lerner (1988) at a slightly higher temperature (309 K).

Table II: Spin–Spin Coupling Constants for the *Eco*RI Duplex[a]

base	$^3J_{1'2',2''}$	$\sum_{1'}$ (Hz)	$\sum_{2'}$ (Hz)	f_s	P_s
Cyt 1	nd	14.5 (14.3)	28	0.8 (0.79)	170
Gua 2	9.4, 6.0	15.4 (15.4)	nd	0.98 (0.98)	nd
Cyt 3	nd	14.7 (15.0)	28	0.83 (0.90)	180
Gua 4	9.5, 5.5	15.0	28	0.90	150
Ado 5	9.6, 6.0	15.6 (15.4)	26	0.98 (0.98)	185
Ado 6	nd	14.5	nd	0.75	nd
Thy 7	nd	15.1	29	0.9	162
Thy 8	9.6, 6.1	15.8 (15.4)	28	0.95 (0.93)	180
Cyt 9	9.1, 6.0	15.0	29	0.86	162
Gua 10	nd	15.3	nd	>0.9	nd
Cyt 11	nd	nd (14.5)	28	0.85 (0.8)	
Gua 12	nd	15.1	nd	0.9	

[a] $^3J_{1'2',2''}$ coupling constants were determined from resolution-enhanced one-dimensional experiments. Otherwise, sums of coupling constants were determined from cross sections of the HOHAHA and DQF-COSY experiments. Values in parentheses refer to coupling constants determined in the *Eco*RI-berenil complex. Errors on $^3J \approx \pm 0.5$ Hz and on $\sum_{2'} \approx \pm 1$ Hz. nd, not determined.

Table III: Apparent Distances for the H1′–H4′ Vectors in the *Eco*RI Duplex[a]

base	dist (nm)	P_s (deg)	base	dist (nm)	P_s (deg)
Cyt 1	>0.33	>160	Thy 7	0.28	130
Gua 2 + Gua 10	0.325	170	Thy 8	0.295	140
Cyt 3	0.27	120	Cyt 9	>0.3	>160
Gua 4	0.32	170	Cyt 11	>0.3	>160
Ado 5	0.29	130	Gua 12	0.3	160
Ado 6	0.295	140			

[a] Apparent distances were determined from NOESY spectra recorded with a mixing time of 50 ms. Cross-peak intensities were normalized to the intensity of the same H1′ to H2″ cross peak, assuming a distance of 0.23 nm. These distances represent lower limits to the true distance, as the relaxation rate of H2″ is much greater than that of H4′. P_s was determined according to the distance, assuming $\phi_m = 37°$.

The derived values of P_s in some cases differ radically from those reported by Nerdal et al. (1989). For example, residue G2 was reported to have $P_s = 252°$. The value of $\sum_{1'}$ for this phase angle is about 10.4 Hz (Rinkel & Altona, 1987), compared with the measured value of 15.4 ± 0.5 Hz. We conclude that the conformation of the sugar attached to G2 reported by Nerdal et al. (1989) is in error. Also, some pseudorotation phase angles were reported to be near 90°, corresponding to O4′ endo. However, in this conformation, the distance H1′–H4′ is at a minimum (ca. 0.25 nm; van de Ven & Hilbers, 1988) and should therefore give relatively intense NOEs. Indeed, extensive simulations show that these NOEs are not greatly affected by spin diffusion, so that reasonably reliable distances can be estimated from NOE intensity ratios at short mixing times. We have used the ratio of the intensities of the H1′–H4′ to H1′–H2″ NOEs ($r = 0.23$ nm) to estimate the H1′–H4′ distance. Because H2″ relaxes faster than H1′, this ratio provides distances that are shorter than the true ones, though the error is relatively small under the conditions of these experiments. The estimated distances are given in Table III, together with the appropriate range of the pseudorotation

Table IV: Properties of Base Protons in the *Eco*RI Duplex[a]

proton	$d\delta/dT$ (ppb/K)	R_2 (s^{-1})	R_1 (s^{-1})	$\sigma(6,5)$ (s^{-1})
Cyt 1 H6	−1.0	nd	2.1	−0.68
Cyt 1 H5	0.27	nd	nd	
Gua 2 H8	−1.1	5.7	nd	
Cyt 3 H6	−1.3	nd	3.3	−0.77
Cyt 3 H5	−0.2	nd	nd	
Gua 4 H8	−1.8	7.8	2.9	
Ado 5 H8	−2.1	9.3	5.1[b]	
Ado 5 H2	2.3	3.8	nd	−0.13[c]
Ado 6 H8	−1.5	9.3	5.1[b]	
Ado 6 H2	0.7	3.0	nd	
Thy 7 H6	−2.5	15.0	3.7	
Thy 8 H6	−1.0	15.6	4.1	
Cyt 9 H6	−0.7	nd	4.0	−0.7
Cyt 9 H5	1.17	nd	nd	
Gua 10 H8	−1.3	7.8	2.6	
Cyt 11 H6	−1.5	nd	4.0	−0.73
Cyt 11 H5	−0.2	nd	nd	
Gua 12 H8	−1.3	5.7	nd	

[a] Temperature coefficients were obtained from resolution-enhanced spectra recorded from 283 to 313 K. R_2 and R_1 were determined as described under Materials and Methods. $\sigma(6,5)$ is the cross-relaxation rate constant for the Cyt H6–H5 vectors determined from NOE buildup curves. nd, not determined. [b] Ado 5 H8, Ado 6 H8 overlapping. [c] Cross-relaxation rate constant Ado 5 H2 to Ado 6 H2.

phase angle, P. The majority of these distances exceed 0.3 nm, which requires that $P > 144°$ (van de Ven & Hilbers, 1988). The exceptions are the residues Cyt 3 and Thy 7, which are consistent with phase angles near 120°. Bax and Lerner (1988) give phase angles of 150° and 124°, respectively, compared with values of 93° and 139° given by Nerdal et al. (1989). Further, at a mixing time of 50 ms, the NOEs H2″–H4′ are exceedingly weak, which is also consistent with the dominant pucker lying well within the south domain. Hence, the coupling constant data and the conformationally sensitive intrasugar NOE intensities are consistent with a relatively small range of pseudorotation phase angles (in the interval 130–180°), with at most a modest admixture of north conformations (Bax & Lerner, 1988). We note that the extreme puckers found by Nerdal et al. (1989) were for those residues where the least number of accurate, independent distances can be measured, owing to significant peak overlap (cf. Table I). We conclude that the precise value of P is difficult to determine. However, as both intra- and internucleotide NOE intensities are quite insensitive to the value of P in the south domain, the determination of the other conformational parameters is not significantly compromised by the imprecision of P (Lane, 1990).

Correlation Time. The overall tumbling time was determined at 303 K by measuring the cross-relaxation rate constants for the Cyt H6–H5 vectors (Lane et al., 1986). The NOE time courses were obtained by irradiating each Cyt H6 resonance in turn for 75, 150, 250, 500, and 750 ms. The value of the correlation time determined from the cross-relaxation rate constants of all four cytosine residues was 3.0 ± 0.1 ns. This value is close to that expected for a rigid ellipsoid of axial ratio about 1.6:1, according to the Stokes–Einstein equation (Lane et al., 1986). We have also measured relaxation rate constants for resolved base protons, which are given in Table IV. The reciprocal spin–lattice relaxation rate constants (R_1) are useful for normalizing NOESY intensities (Mirau, 1988) and also show that the bases reside in magnetically similar environments.

^{31}P NMR. The phosphate resonances of the dodecamer have been assigned by Ott and Eckstein (1985) and the T_1 and $\{^1H\}^{31}P$ NOEs have been measured at 303 K by Patel et al. (1983). We have confirmed the assignments of Ott and Eckstein (1985) by ^1H–^{31}P correlation spectroscopy (data not shown), which also confirms the assignments of the H4′ resonances (Table I). We have also measured the R_1, R_2, and NOE values at two magnetic field strengths (4.7 and 11.75 T). The values are given in Table V. The values of R_1 at 4.7 T are similar to those reported by Patel et al. (1983), though in our hands the NOEs were insignificant. At 4.7 T, the relaxation rate is only about 40% dipolar, and for a correlation time of 3 ns, the NOE would be expected to be only about 1.02 for a rigid body (Forster & Lane, 1990). The lack of a significant NOE at the lower field strength is consistent with the absence of fast, large-amplitude internal motions affecting the P–H vectors. Measurements of R_1 and R_2 were also made at 202.4 MHz, as reported in Table V. At the higher field, the relaxation is at least 90% CSA, when the ratio R_2/R_1 becomes approximately (Williamson & Boxer, 1989)

$$R_2/R_1 = 7/6 + 2\omega_p^2\tau^2/3 \quad (3)$$

where ω_p is the phosphorus frequency in radians per second and τ is the correlation time. By use of the data in Table V, correlation times ranging from 3.4 to 4.3 ns are found. These values are significantly higher than the correlation time for the cytosine H6–H5 vectors but may reflect the larger correlation time for end-over-end tumbling, which is about 3.9 ns for the dodecamer (see above).

The function $R_2 - 0.5R_1 = \Delta R$ is given by (Forster & Lane, 1990)

$$\Delta R = 88.88\xi^2\omega_p^2\tau^2 J(0) + 9.348\sum r^{-6}\{2J(0) + 3J(\omega_H)\} \quad (4)$$

where ξ is the CSA, defined as the product of the shift anisotropy $\Delta\sigma$ and the asymmetry factor. The effective value of r, which is summed over all P–H vectors in the molecule, is about 0.21 nm on the basis of models of B-DNA. The value of ξ then obtained is about 140–150 ppm, which is similar to estimates made in other systems (Williamson & Boxer, 1989; Forster & Lane, 1990). Using these values as initial estimates, the R_1, R_2, and NOE at the two field strengths were used to refine the values of τ, ξ, and r_{eff}. A perfect fit to all the data could not be obtained by assuming a rigid body. However, if the dipolar contribution (which is significant only at 4.7 T)

Table V: ^{31}P Relaxation Data at 81 and 202.4 MHz for the *Eco*RI Duplex at 303 K[a]

		81 MHz			202.4 MHz				
δ ppm	phosphate	R_1 (s^{-1})	R_2 (s^{-1})	ΔR (s^{-1})	R_1 (s^{-1})	R_2 (s^{-1})	ΔR (s^{-1})	τ_{app} (ns)	ξ (ppm)
−17.20	C1pG,C9pG	0.58	2.53	2.24	0.75	10.0	9.6	3.3	143
−17.30	C3pG	0.60	2.80	2.50	0.69	9.4	9.0	3.4	136
−17.35	C1pG,G10pC	0.61	2.61	2.31	0.72	11.4	11.0	3.7	144
−17.45	G4pA,G2pC	0.63	2.85	2.54	0.69	12.0	11.7	3.8	144
−17.60	A5pA,T8pC	0.69	3.27	2.92	0.70	14.0	13.7	4.2	150
−17.71	A6pT,T7pT	0.75	3.26	2.89	0.75	15.9	15.5	4.3	158
								mean 3.8 ± 0.37	146 ± 7

[a] ^{31}P assignments were taken from Ott and Eckstein (1985) and referenced to external methylene diphosphonate. τ_{app} was calculated from R_2/R_1 and ξ from ΔR as described in the text. Error is ca. 10% on τ_{app} and ξ.

is scaled by an order parameter S^2, then an acceptable fit can be found for each phosphate by using an overall correlation time of 3.5 ns. The mean value of ξ was 147 ± 6.4 ppm, with a range of only 20 ppm. Similarly r_{eff} varied from 0.204 to 0.23 nm, with a mean 0.22 ± 0.01 nm. To fit all the data, the value of S^2 ranged from 0.7 to 1.0, indicating the absence of large-amplitude fluctuations in the subnanosecond time scale. However, both the CSA and the apparent correlation time for C3pG4 and C9pG10 are significantly smaller than on average, whereas the CSA and apparent correlation time for A6pT7 and T7pT8 are significantly larger than average (Table V). According to Ott and Eckstein (1985) and Gorenstein et al. (1988), these positions also have anomalous chemical shifts consistent with sequence-dependent variations in the C–O–P backbone angles. Differences in these angles along the sequence would be expected to affect the CSA tensor and possibly the apparent correlation time in an anisotropic rotor if this also changes the orientation of the principal axis of the CSA tensor with respect to the long axis of the duplex. Although it is not possible to analyze these data in greater detail, they do point to the presence of different backbone angles at the C3–G4/C9–G10 and A6–T7 steps.

Nerdal et al. (1989) also derived rather different conformations for these steps, which, as they point out, correlate with the kinks seen in the complex of the dodecamer with the *Eco*RI restriction endonuclease (McClarin et al., 1986). Nerdal et al. (1989) suggested that the kinks observed in the complex preexist in solution. To some extent, our results support this idea. However, according to Kim et al. (1984), the *Eco*RI restriction endonuclease causes a 25° unwinding of the helix, but only when bound to the specific restriction site. It seems unlikely that an already severely underwound helix, as proposed by Nerdal et al. (1989) (average twist = 20°, 18 base pairs per turn), would be yet further unwound by binding the enzyme. An alternative possibility is that the DNA is more flexible at these positions, as a consequence of the local sequence, and the enzyme either selects the appropriate (low population) conformer from a broad distribution or causes sequential changes in conformation in a multistep binding process. For either mechanism, the properties of the DNA helix at these positions are required to differ significantly from those at other positions.

NOEs. NOESY spectra were recorded at 50, 100, 150, and 200 ms with a 3-s recycle time to allow spin–lattice relaxation. The cross-peak intensities were normalized to unit spin intensity at each mixing time as described under Materials and Methods. In addition, one-dimensional NOE time courses were obtained on irradiation of each of the four Cyt H6 resonances and for the Ado 5 H2–Ado 6 H2 pair.

The relative intensities of the intranucleotide NOEs, H8/6 to H1′, H2′, H2″, and H3′, are consistent with the glycosidic torsion angle, χ, being anti for all residues, and the internucleotide NOE connectivities indicate a right-handed screw. As the coupling constants show that the dominant pucker is near C2′ endo, the dodecamer belongs to the B family of conformations in solution. The nucleotide conformations were found by setting the pseudorotation phase angles to those given in Table III and optimizing χ for several values of the fraction of the south conformation, f_s, from 0.6 to 1.0 (cf. Table II), starting with data at the shortest mixing time and gradually including the data from longer mixing times. This minimizes the effects of incorrect T_1 values. The reciprocal T_1 values of the observed spins were also optimized after each cycle of optimization of χ. Finally, χ, f_s, and T_1 were simultaneously optimized from the best values found in the previous cycles.

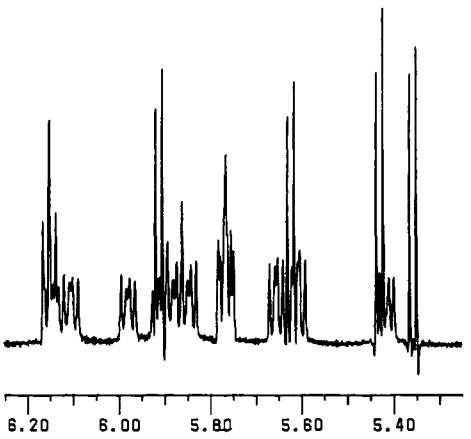

FIGURE 1: Partial (H1′ region) ^{1}H NMR spectrum of the *Eco*RI duplex, d(CGCGAATTCGCG)$_2$. The spectrum was recorded at 303 K as described under Materials and Methods. The free induction decay was zero-filled to 32 k points (resolution = 0.3 Hz/point) and enhanced by using a Lorentz-to-Gauss transformation with LB = −3 and GB = 0.3.

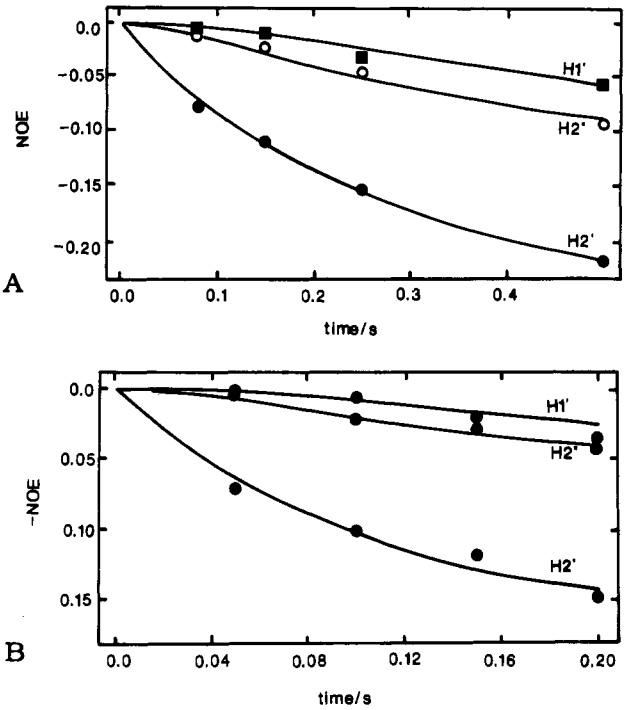

FIGURE 2: Least-squares fits to the NOE intensities of Cyt residues of the *Eco*RI duplex. Least-squares optimization of the nucleotide conformation to the observed NOEs was done with NUCFIT as described under Materials and Methods. The pseudorotation parameters were obtained from coupling constants as given in Table II. (A, Top) Data from truncated one-dimensional NOE experiments for Cyt 11 showing best-fit regression lines from the parameters given in Table VI. (B, Bottom) Data from NOESY experiments for Cyt 9 with best-fit lines from the data in Table VI.

Because of the strong dependence of the NOE intensities on χ, the glycosidic torsion angle is well-determined, whereas f_s is relatively poorly defined. Fortunately, the values of χ and f_s are essentially independent parameters (Lane, 1990). Figure 2A shows the a least-squares fit to the data obtained for Cyt 11 with one-dimensional data. A fit for the NOESY data for Cyt 9 is shown in Figure 2B. In these calculations, order parameters for the sugar proton–proton vectors were determined from NOESY spectra at 50 ms for H1′ to H2″/H2′ and H3′ to H2′/H2″. The order parameters were about 0.75 for the H1′–H2″ vectors and >0.9 for the H2′–H2″ vectors, in agreement with Reid et al. (1989). Interestingly, the order

Table VI: Intranucleotide Conformations for the *Eco*RI Duplex[a]

base	χ (deg)	f_s	R
Cyt 1	−122	0.9	0.24
	(−124)	0.77	0.18
Gua 2	−100	1.0	0.11
Cyt 3	−116	0.9	0.10
	(−114)	0.8	0.15
Gua 4	−112	0.95	0.17
Ado 5	−110	1.0	0.18
Thy 7	−115	1.0	0.17
Thy 8	−117	1.0	0.09
Cyt 9	−114	0.97	0.09
	(−115)	0.86	0.05
Gua 10	−104	0.99	0.14
Cyt 11	−108	0.9	0.15
	(−117)	0.92	0.08
Gua 12	−112	1.0	0.07
mean	−113 ± 6°		

[a] χ is the glycosidic torsion angle, f_s is the fraction C2′ endo and R is the mean absolute fractional error. Pseudorotation phase angles were taken from Table II or otherwise set to 162° for purines and 144° for pyrimidines. Values in parentheses were obtained from one-dimensional NOE progress curves, while all others were determined from time-dependent NOESY data. The statistical error on χ = ±3° and on f_s = ±0.1.

parameters for Cyt 1 were all significantly smaller than for the other residues, suggesting significant internal mobility of the 5′-terminal base, as observed for other oligomers (Lane & Forster, 1989). These values are very similar to those previously observed in unrelated sequences (Lefèvre et al., 1987; Lane & Forster, 1989).

We note also that the corresponding intraresidue NOE intensities in Cyt 3, Cyt 9, and Cyt 11 are identical, within experimental error, for both one- and two-dimensional experiments. Therefore, the conformations of these nucleotides must be very similar. The conformational parameters for the nucleotide units are given in Table VI. Note that because the NMR spectra show only a single set of resonances, the two strands are taken as equivalent. The glycosidic torsion angles of Cyt 3, Cyt 9, and Cyt 11 are very similar (≈−113°), whereas that of Cyt 1 is larger (−123°). The determination of the glycosidic torsion angles for the cytosine residues using one- and two-dimensional data agree well, indicating that this parameter is well determined by the data. There are significant differences between several of the glycosidic torsion angles determined for the solution state and those reported for different crystal conditions. We note that the glycosidic angles for the same nucleotide in the two strands in many cases differ by 10–20° in the crystal state and by similar amounts between different crystal conditions (Fratini et al., 1982). It is not clear how much these differences between the solution and crystal states relate to crystal packing effects and to the necessary assumption of equivalence of both strands in the solution state. The glycosidic torsion angle of Cyt 3 is well determined by the NOE data, which is completely inconsistent with the value of 135° in the crystal state of the native dodecamer. We also find significant differences between glycosidic torsion angles (where measurable) and those reported by Nerdal et al. (1989), which we attribute to propagation of errors from incorrect sugar puckers and possibly systematic errors in the distances used in their initial distance geometry calculations. However, the main point of the present article is to determine changes in conformation induced by complexation with a ligand.

NOE time courses were also generated by irradiating in turn each of the imino proton resonances at 298 K (the correlation time at 298 K in H_2O is equal to that in D_2O at 303 K), to provide additional restraints for the determination of the helical parameters. As the interproton vectors are essentially parallel to the helix axis, the appropriate correlation time for these vectors is equal to that for end-over-end tumbling. For an axial ratio of 1.6:1, this correlation time is 3.8 ns at 303 K. We obtain distances between imino protons of 0.36 ± 0.02 nm for Gua 2–Cyt 3, 0.38 ± 0.03 nm for Cyt 3–Gua 4, 0.39 ± 0.03 nm for Gua 4–Ado 5, and 0.35 ± 0.02 nm for Ado 5–Ado 6. From the dependence of the line width on temperature (not shown), the extent of exchange with solvent under our solution conditions is small for the internal base pairs. However, given the lower accuracy of the NOE measurements for these protons, the derived distances are used only to limit the search in the helical rise, which must be smaller than the upper limit of the NH–NH distance.

Helical Parameters. At least six parameters are needed to describe the relative orientation of one base pair with respect to its neighbor. These can be the helical rise (translation along the z axis), shift (translation along the x axis defined by the C8–C6 vector of a base pair), slide (translation along the y axis), helical twist (rotation around z), roll (rotation around x), and tilt (rotation around y). In addition, the base pairs may show propeller twisting, which requires another parameter. In general only three to four internucleotide NOEs per strand are observed, for a total of six to eight inter-base-pair NOEs. As the inter-base-pair NOEs are not all linearly independent (Lane, 1990) and tend to be relatively weak, the problem may be underdetermined. We have searched conformational space for two base pairs at a time, initially setting the nucleotide conformations to those found above. The search was constructed by setting up a grid of values for the helical rise, tilt, slide, shift, and roll. At least 200 conformations were searched for each two-base-pair fragment (consisting of 30–40 protons) with least-squares optimization of the helical twist and apparent T_1 values for each data set (with the exception of those for base protons measured experimentally, cf. Table IV), in the manner described above for the nucleotide conformations. Optimized conformations were retained for which the value of R is close to that expected for random error (0.1–0.15 for the data presented here) and minimal van der Waals violations and where distances between C3′(i) and C5′(i+1) remain within the allowed limit of 0.52 nm. These conformations were further refined by least-squares minimization with free variation of all parameters. In this procedure, the final result gives quite high precision for the helical twist, moderate precision for the tilt angle, and substantially lower precision for the other parameters (Lane, 1990). For this reason, and because of the nature of the sampling process, the majority of the parameters can only be assigned a range of values that produce NOE intensities consistent with the data, while not causing severe van der Waals violations. Figure 3 shows a fit for the step Gua 2–Cyt 11/Cyt 3–Gua 10. This step is the best defined of all because of the larger number of observed NOEs, including interimino proton NOEs. Nevertheless, while the twist and tilt are reasonably well-determined (statistical errors of about ±3° and ±5°, respectively), the other parameters are not so well-determined. Indeed, the base-pair roll could be varied from 0 to −20° with minimal influence on the determination of the other parameters or on R. This agrees with previous simulations that show that internucleotide NOEs are rather insensitive to the base-pair roll (Lane, 1990). Table VII presents the refined parameter estimates for the dodecamer.

The agreement between fits obtained for one- and two-dimensional NOE data is excellent, suggesting that when suf-

Table VII: Helical Parameters for the *Eco*RI Duplex[a]

base step	roll (deg)	tilt (deg)	twist (deg)	shift (nm)	slide (nm)	rise (nm)	*R*
C1G12/G2C11	−10/−20	0/−5	45 (43/53)	0/0.05	0/.1	0.33/0.39	0.146
G2C3/G10C11	0/−20	0/−5	35 (30/39)	0/−0.05	0/−0.05	0.31/0.37	0.15
G2C3/G10C11*	0/−20	0/−6	35 (27/38)	0/−0.05	0/0.05	0.31/0.37	0.097
G2C3 (+B)*	0/−10	0/−5	35 (33/40)	0/0.05	0	0.3/0.37	0.12
C3G4/C9G10	−10/−30	0/−5	35 (32/43)	0/−0.05	0/−0.1	0.34/4.1	0.08
G4A5/T8C9	0/−20	0	36 (31/41)	0/−0.25	−0.05/−0.1	0.35/0.4	0.16
G4A5/T8C9*	0	0	41 (37/46)	0/−0.1	0/−0.1	0.38 ± 0.03	0.14
A5A6/T7T8	0/−20	0/−10	30 (28/38)	0/−0.5	0.05/−0.1	0.3/0.39	0.095
A6T7/A6T7	0/−30	0	36 (24/37)	0	−0.1/0.2	0.32/0.41	0.16
A6T7 (+B)*	0/−30	0	39 (31/42)	0/−0.05	0/−0.05	0.32/0.41	0.108
			mean 36.8 ± 4.6°				

[a] Helical parameters were determined from one- and two-dimensional NOE time courses by combined parameter-space searching and least-squares optimization, as described in the text. The parameters are given as ranges consistent with the data according to the criteria described in the text, except the twist angle, which is given as the best value, with the range in parentheses. For each base pair, at least 200 conformations were searched. An asterisk denotes solutions obtained from one-dimensional NOE data sets; +B denotes values in the presence of berenil.

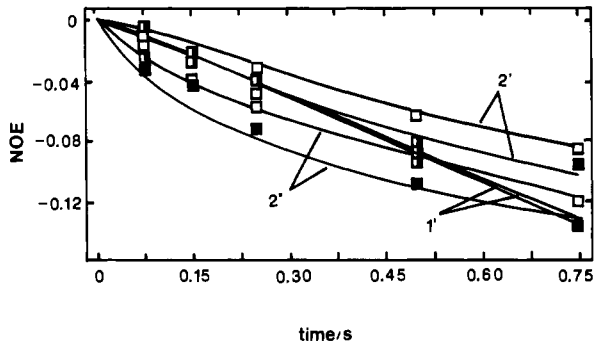

FIGURE 3: Determination of the conformation of the base-step Gua 2–Cyt 11/Cyt 3–Gua 10 in the *Eco*RI duplex. Optimal conformations consistent with the data were found by combined least-squares refinement with conformational space searching using NUCFIT. The data are shown for the one-dimensional truncated NOE experiments for irradiation of Cyt 3 H6 and Cyt 11 H6. The lines are drawn for a rise of 0.35 nm, a helical twist of 34.4°, a roll angle of 10°, a tilt angle of 0°, a shift of 0 nm, and a slide of 0.1 nm. The *R* factor was 0.083. (□) NOEs between Cyt 3 H6 and Gua 2 protons; (■) NOEs between Cyt 11 H6 and Gua 10 protons.

ficient data are available, the most sensitive parameters are well-determined. However, in some steps, data were lacking owing to spectral overlap (Ado 5–Ado 6) or because of low intensity (e.g., Cyt 3–Gua 4). Under these circumstances, the values of the helical parameters are uncertain, and the problem is underdetermined. There are sequence-dependent effects on the helical parameters, particularly the helical twist. The average twist is 36.5 ± 5°, which translates to 9.8 ± 1 base pairs per turn. For comparison, we note that the structures generated by Nerdal et al. (1989) imply an average helical twist of 20 ± 8° (18 ± 5 base pairs per turn), i.e., significantly underwound, while Fratini et al. (1982) give the average helical twist of 36 ± 4° for the native dodecamer. Our results are more in line with the X-ray diffraction data than are those of Nerdal et al. (1989). The slight overwinding of the helix implied by our results may be a consequence of some twist angles being poorly determined (cf. Cyt 1–Gua 2 and Ado 6–Thy 7); under these conditions the algorithm finds optimal solutions that give slightly overwound structures (Lane, 1990). The helical parameters for Ado 6–Thy 7 are less well-determined than for other steps because the glycosidic torsion angle of Ado 6 was not determined independently; the values given in Table VII were obtained for initial values of χ(Ado 6) ranging from −105 to −120°.

The helical rise is in the range 0.3–0.4 nm. In general the base-pair tilts are small, while base-pair roll angles in some cases can be up to −30°. The base-pair shifts and slides are also in general small. From this information together with the nucleotide parameters, it is clear that the *Eco*RI dodecamer in solution is a member of the B-DNA family of conformations. Unfortunately, because the dependence of the NOE intensities on the base roll is so weak, it is not possible to provide estimates of the propeller twist or give any indication as to whether the helix is straight or bent. This is a limitation of the NMR data sets. It is not possible, therefore, to state with certainty what the absolute accuracy of the structure determination is, which varies from parameter to parameter. Nevertheless, as we are concerned mainly with conformational changes due to ligand binding, it should be possible to place limits on the magnitude of any changes that occur. We note, however, that in a restrained molecular dynamics study, the conformation of a very similar dodecamer was linear and close to that of classical B-DNA, with the average helical twist about 35° and small values of the roll and tilt angles (Gronenborn & Clore, 1989), and that the average conformation is similar to those derived from crystallographic determinations of the same oligomer (Fratini et al., 1982; Saenger, 1984).

Interaction of d(CGCGAATTCGCG)$_2$ with Berenil. Optical Spectroscopy. We have used optical spectroscopy to characterize the binding of berenil to the *Eco*RI dodecamer under solution conditions similar to those used for the NMR experiments. Figure 4A shows a difference spectrum for the complex in the visible region of the spectrum. Binding is characterized by a red shift of the absorption spectrum for the ligand; Figure 4B shows the CD difference spectrum. Berenil itself has no detectable ellipticity at these concentrations, so that the positive bands in the region 350–380 nm must be induced Cotton effects arising from the interaction of the chromophore with the dissymmetric environment of the DNA. The maximum ellipticity produced was 2150 deg M^{-1} cm^{-1}. In the near-ultraviolet, the normally conservative spectrum of the DNA is perturbed. However, as berenil has a weak absorption band near 260 nm, it is not clear whether the change is due to a change in the conformation of the DNA, the induced Cotton effects in the ligand, or a combination of both. Titrations of 2.2 μM duplex with berenil, using the bands at 370, 380, and 280 nm, showed that the dissociation constant, K_d, for the interaction is 1 ± 0.1 μM at 298 K (Figure 4C). Hence, at concentrations of duplex used for the NMR experiments (ca. 0.8 mM in duplex), the binding is effectively stoichiometric; at equal concentrations of ligand and DNA, the complex accounts for >95% of the molecules present.

NMR Spectroscopy. Figure 5 shows part of a 150-ms phase-sensitive NOESY experiment of the berenil–dodecamer complex. There are numerous changes in chemical shift in the complex, but all of the protons could be assigned (cf. Table I). Interestingly, the chemical shift degeneracy of the ligand

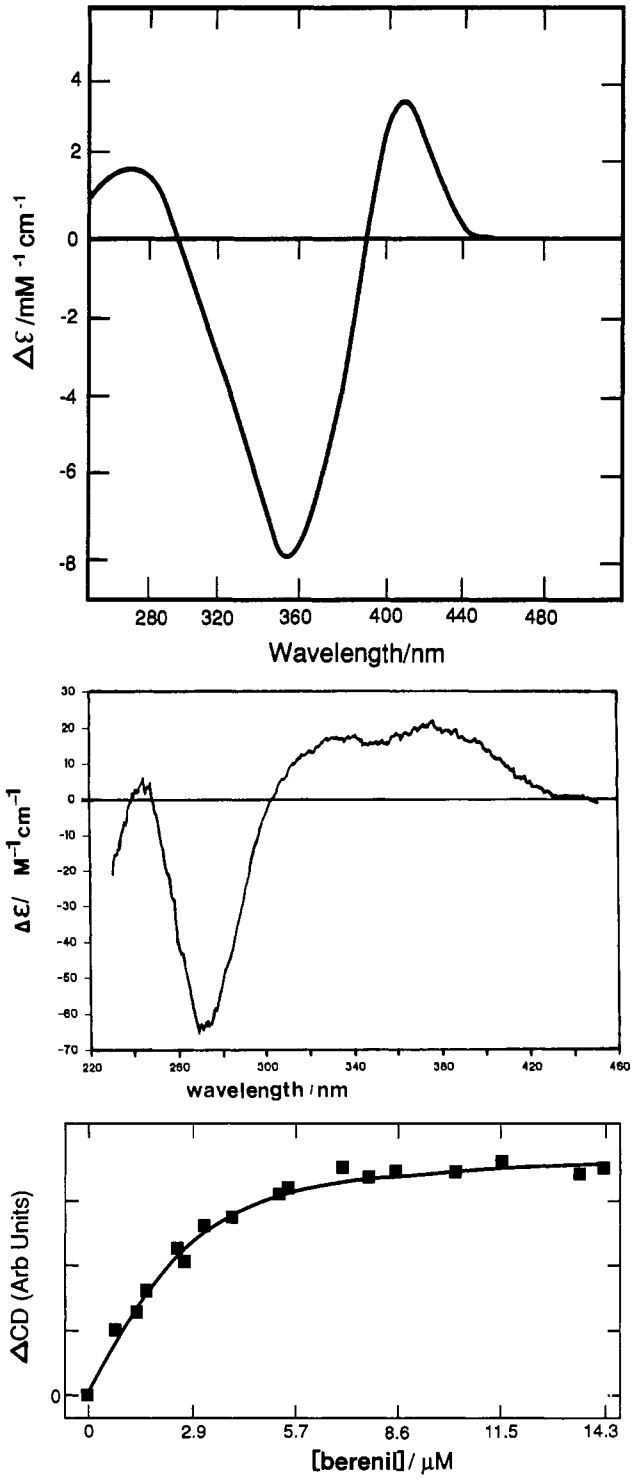

FIGURE 4: Optical spectroscopy of the interaction of the *Eco*RI duplex with berenil. Absorbance and CD spectra were recorded as described under Materials and Methods. The buffer was 5 mM sodium phosphate and 100 mM KCl, pH 7.0 at 298 K. (A, Top) Absorbance difference spectrum generated with 2 μM (duplex) DNA and 30 μM berenil. (B, Middle) CD difference spectrum. The DNA concentration was 2.2 μM and the berenil concentration was 30 μM. (C, Bottom) CD titration of berenil with the dodecamer. The dodecamer (2 μM) was titrated with increasing concentrations of berenil. The data were analyzed by least-squares regression for a single site. The line is the best-fit line with K_d = 1 ± 0.1 μM.

protons is not lifted in the complex, though the resonances are shifted about 0.15 ppm downfield and become rather broad. This may be due to a slight asymmetry in the chemical shifts. Integration of a one-dimensional spectrum (not shown) indicates that the stoichiometry of the complex is 1.2 ± 0.2 mol

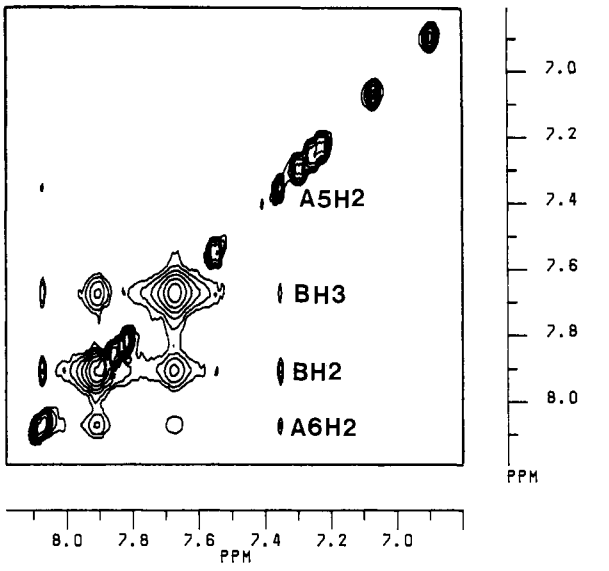

FIGURE 5: Partial NOESY spectrum of the *Eco*RI–berenil complex. The complex was prepared as described under Materials and Methods. The phase-sensitive NOESY spectrum was recorded at 303 K with a mixing time of 150 ms, and the data were processed by using a 60°-shifted sine-squared function in both dimensions. Base protons and berenil protons are given showing connectivities between the resonances of the ligand (BH2 and BH3) and the H2 resonances of Ado 5 and Ado 6.

of ligand to 1 mol of duplex. Figure 6 shows the changes in chemical shifts on forming the complex for the base H8/H6/H5/Me protons (major groove), the H1′ resonances, and the H2′/H2″ resonances (minor groove). The most striking feature of the shifts is that they are localized to at most four bases, namely, Ado 6, Thy 7, Thy 8, and Cyt 9; the chemical shifts of the remaining resonances change by <0.05 ppm. The largest shifts are found for the H1′ resonances, followed by the H2′/H2″ resonances (all in the minor groove), while the smallest changes are found for the H8/H6 resonances (major groove). The H2 resonances of the two adenines also show large shifts, with A6 H2 0.46 ppm downfield and A5 H2 0.14 ppm downfield. These protons are also found in the minor groove. It seems likely that a significant fraction of the shifts of resonances in the minor groove arise from proximity to the aromatic ring systems of the ligand. However, the changes in shift of resonances in the major groove suggest that the conformation of the DNA may be altered locally in the segment Ado 6–Cyt 9. Although there is no lifting of the chemical shift degeneracy of sequence-related protons, we cannot rule out local differential conformations in the two strands or rapid exchange between two similar sites.

The phosphorus chemical shifts in the complex were determined by correlation spectroscopy (data not shown), and the changes are also shown in Figure 6. The phosphorus chemical shifts are significantly perturbed for the phosphodiesters A6pT7, T7pT8, and T8pC9, which is consistent with the ligand lying in the minor groove and close to the phosphates.

NOEs were also observed between the ligand resonances to Ado 5 H2, Ado 6 H2, Thy 7 H1′, and Thy 8 H1′. As all of these protons are in the minor groove, we conclude that the ligand also sits in the minor groove.

We have recorded one-dimensional time courses with irradiation of the H6 resonances of Cyt 3, Cyt 9, Cyt 11, Thy 7, and Thy 8, the H2 resonances of Ado 5, and the broad ligand resonances. The correlation time for the cytosine H6–H5 vectors is 3.35 ± 0.2 ns, which is very similar to that determined for the free DNA (see above). Hence, there are no

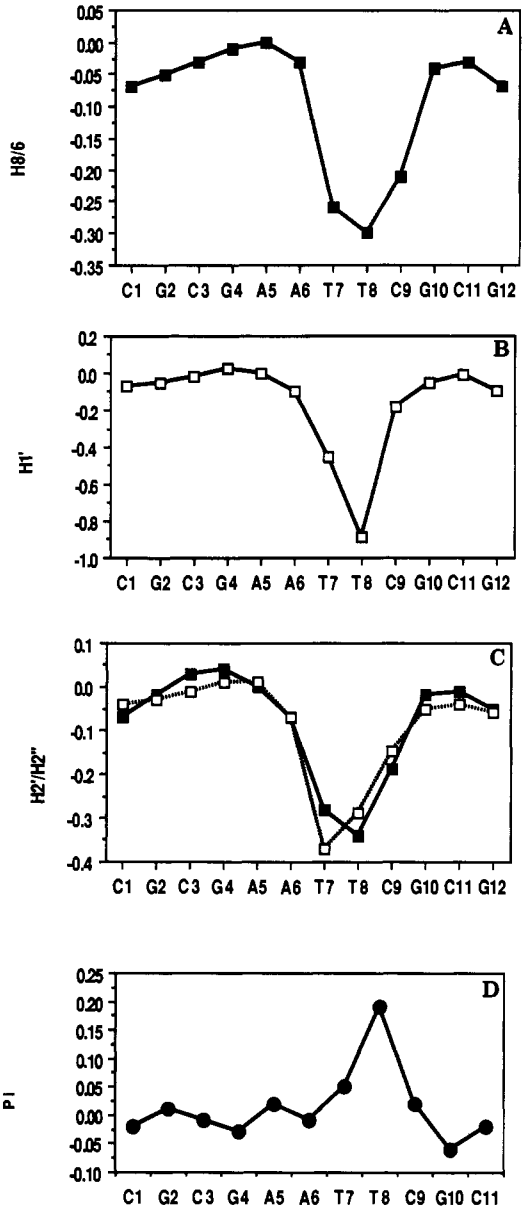

FIGURE 6: Chemical shift differences between the free *Eco*RI and the *Eco*RI–berenil complex. Proton data were taken from Table I. Phosphate chemical shifts were determined by correlated spectroscopy as described in the text. Chemical shift differences are those in the DNA–berenil complex minus those in the free duplex: (A) H8/H6; (B) H1′; (C) (■) H2′, (□) H2″; (D) phosphates.

massive changes in the conformation of the molecule that change the rotational friction coefficients. The coupling constants, where measurable, indicate that there are no dramatic changes in the sugar conformations (Table II). Similarly, relative NOE intensities at short mixing times for base to H2′ indicate that the glycosidic torsion angles are also not significantly affected by the binding. Figure 7 shows the best fit to the one-dimensional NOE data for residue Thy 7.

In the free dodecamer, the distance between the H2 protons on Ado 5 and Ado 6 can be obtained from the cross-relaxation rate constant. These protons are quite isolated and therefore form a two-spin system. From the NOE time course, we obtain a value for the cross-relaxation rate constant of −0.13 s^{-1} (see Table IV). From a correlation time of 3.8 ns (appropriate for vectors parallel to the long axis of the dodecamer, see above), the distance between these protons on the free DNA is 0.35 ± 0.02 nm. In the presence of berenil, these protons can no longer be treated as an isolated pair of spins

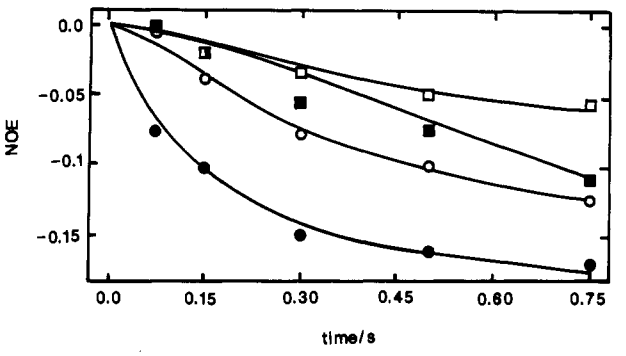

FIGURE 7: Determination of the conformation of Thy 7 in the presence of berenil. Truncated one-dimensional NOEs from H6 were recorded as described in the text: (□) H1′; (●) H2′; (○) H2″; (■) H3′.

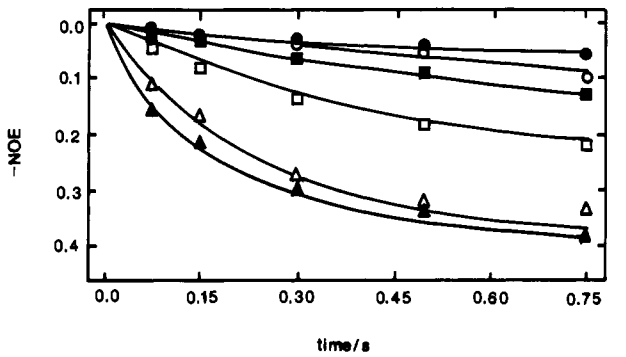

FIGURE 8: Determination of cross-relaxation rate constants for the *Eco*RI–berenil complex. Cross-relaxation rate constants were determined from one-dimensional NOE time courses as described in the text. The lines are regression fits for cross-relaxation rate constants given in Table VII. (●) Ado 5 H2–Ado 6 H2; (○) Ado 5 H2–BH3; (■) BH3–Ado 5 H2; (□) BH3–Ado 6 H2; (△) BH2–BH3; (▲) BH2–Ado 6 H2.

because of the significant NOEs between the aromatic protons of the ligand and both Ado H2 protons. We have therefore used a multispin treatment to fit the NOE time courses simultaneously for the NOEs obtained on irradiation of Ado 5 H2 and both ligand resonances, using a modification of NUCFIT. In these calculations, NOEs were recorded at five irradiation times (75, 150, 300, 500, and 750 ms) for irradiation of the three protons in turn. NOEs were observed between all protons, giving a total of 35 NOE intensities to be used in the calculation. Figure 8 shows the fits obtained by using the multispin calculation. All six cross-relaxation rate constants, and the four spin–lattice relaxation rate constants were fitted. A wide range of initial values of the parameters was used, including those determined from two-spin fits. Some initial sets of parameters converged to poor minima as judged by the final value of R and visual inspection of the fit to the data. Only fits for which $R < 0.1$ and good visual agreement of the calculated time courses with the observed NOEs were retained. Five of the six cross-relaxation rate constants were reasonably well determined (relative error less than 20%). Only the cross-relaxation rate constant for Ado 6 H2–BH2 was poorly determined (relative error = 46%), presumably because a large fraction of the observed NOE arises from indirect magnetization transfer. The cross-relaxation rate constants and derived apparent distances are given in Table VIII.

From the cross-relaxation rate constant for Ado 5 H2–Ado 6 H2 and the correlation time, we obtain a distance of 0.35 ± 0.02 nm in the presence of berenil. This value compares well with that determined in the absence of the drug, 0.35 ± 0.02 nm (see above), and suggests that the orientation of Ado

Table VIII: Summary of Cross-Relaxation Rate Constants for the *Eco*RI–Berenil Complex[a]

H_A	H_B	$-\sigma$ (s^{-1})	r_{app} (nm)
Cyt 3 H6	Cyt 3 H5	0.89	0.246
Cyt 9 H6	Cyt 9 H5	0.76	0.246
Cyt 11 H6	Cyt 11 H5	0.89	0.246
Ado 5 H2	Ado 6 H2	0.15	0.33
*Ado 17 H2	BH2′	0.12	0.34
*Ado 17 H2	BH3′	0.22	0.31
Ado 6 H2	BH2	0.46	0.27
*Ado 18 H2	BH2	0.46	0.27
*Ado 18 H2	BH2′	0.46	0.27
Ado 6 H2	BH3	2.5	0.21
BH2(2′)	BH3(3′)	1.7	(0.23)
*Thy 19 H1′	BH2	0.56	0.265
Thy 8 H1′	BH2	0.35	0.285
Thy 8 H1′	BH2′	0.35	0.285

[a] Cross-relaxation rate constants connecting Ado 5 H2, Ado 6 H2, and the two ligand resonances were determined from a fit to a four-spin system as described in the text. Other cross-relaxation rate constants were determined from two-spin fits. The distances were calculated for a correlation time of 3.35 ns determined from the cross-relaxation rate constants of the Cyt H6–H5 vectors in the DNA–berenil complex. BH2 and BH3 are the nonexchangeable proton resonances of the ligand. r_{app} is calculated from NOE data by assuming isotropic rotation, which may underestimate distances by up to 5%. Distances are also estimated by assuming symmetry between the strands. Values marked with an asterisk show target distances obtained during the refinement when asymmetry was induced in the binding site (see text). The sequence numbering is as follows:

5′-C1 G2 C3 G4 A5 A6 T7 T8 C9 G10 C11 G12
G24 C23 G22 C21 T20 T19 A18 A17 G16 C15 G14 C13-5′

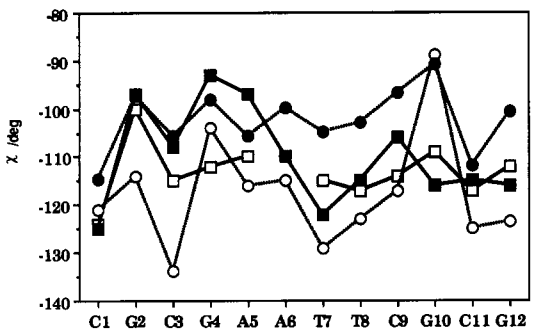

FIGURE 9: Variation of the glycosidic torsion angle in the *Eco*RI duplex in the absence and presence of berenil. Torsion angles (χ) for the crystal state were taken for the native dodecamer (Dickerson & Drew, 1981) and for the complex (Brown et al., 1990), in which the angles for symmetry-related nucleotides have been averaged. The solution values were taken from Tables VI and IX. X-ray: (○) native DNA; (●) complex. NMR: (□) free DNA; (■) complex.

6 with respect to Ado 5 is not greatly affected by ligand binding.

Analysis of the NOESY and one-dimensional NOE intensities and coupling constants in the complex gave the glycosidic torsion angles shown in Figure 9. By comparison with the values in the free DNA (Table VI), it is clear that the conformations of the majority of the nucleotide units are not significantly altered in the complex (i.e., the glycosidic torsion angles change by <5°). Only two residues show any indication of a possible change in nucleotide conformation, namely, residues Gua 4 and Ado 5, where the changes in the glycosidic torsion angles are 19 and 13°, respectively. These residues are at the edges of the binding site and may reflect some rearrangement to accommodate changes in the binding site itself. Unfortunately, the spectral overlap of residues Ado 5 and Ado 6 in the free DNA precluded an analysis of the conformation of Ado 6, so we are unable to determine whether this residue is also affected by binding. Nevertheless, the conformational differences that do appear are quite small. Figure 9 shows a comparison of the glycosidic torsion angles found in solution with and without berenil and also in the native crystal derivative with and without berenil (Dickerson, 1981; Fratini et al., 1982; Brown et al., 1990).

By comparison of the NOE data obtained in one-dimensional NOE experiments in the absence and presence of berenil ligand and independent fitting of the data, it is clear that the conformation of the base step Gua 2–Cyt 3/Cyt 9–Gua 10 is unchanged by binding the ligand; this step is outside the binding site. On the other hand, changes are observed in the base-pair steps in the binding site, in particular Ado 6–Thy 7 and Thy 7–Thy 8. However, even here the changes in conformation are relatively small. This indicates that the ligand can simply slot into the preformed binding site with minimal reorganization.

Molecular Modeling and Energy Minimization. Initial models for the *Eco*RI–berenil complex were generated as described under Materials and Methods with (i) 1:1 DNA–berenil stoichiometry, (ii) the ligand centrally located in the minor groove of a canonical B-DNA at a nominal A6pT7 site, and (iii) the inner concave surface facing the convex floor of the groove. The global B-like DNA conformation was selected on the basis of the derived nucleotide parameters (see above). As the berenil molecule is asymmetric about the triazene (N=N—NH) core, two essentially equivalent models were built in which the ligand was rotated 180° about the central nitrogen atom of the triazene to examine the sensitivity of the DNA binding to ligand orientation. In addition, a model for the free dodecamer was constructed to establish that subsequent restrained molecular dynamics refinement in the absence of the ligand would retain B-like DNA structural integrity.

These structural models were then refined by energy minimization using the X-PLOR program and the recommended three-stage procedure of Brünger (1980), including simulated isothermal dynamic annealing (equilibration) and final conjugate-gradient optimization to reduce strain and bad contacts. The restrained molecular dynamics X-PLOR strategy used has recently been examined (Gronenborn & Clore, 1989). NOE-derived interproton distance restraints and glycosidic dihedral constraints (±5°) were taken from Tables VIII and IX, respectively. Intra- and internucleotide NOE restraints were assigned estimated error ranges of ±0.01 and ±0.015 nm (i.e., ±4%), respectively, while intraligand NOEs were restrained to ±0.01 nm. The error ranges assigned to the DNA–berenil distances were uniformly scaled to ±0.05 nm for interproton distances ≥0.25 nm and ±0.03 nm for distances <0.25 nm (i.e., r_{app} values ±14–19%).

Initially, preliminary structures for the complex were examined by using only the short-range NOE restraints ≤0.27 nm involving the H2 protons of Ado 5 and Ado 6 and the inner face BH2(2′) and BH3(3′) protons of berenil, using the assumption of equivalence for the two strands in the solution state (i.e., Ado 5 ≡ Ado 17 and Ado 6 ≡ Ado 18). Glycosidic torsion constraints were applied equally to both DNA strands, assuming direct equivalence for corresponding nucleotides. Additional NOE restraints and possible proton assignments, together with the longer range interactions, were applied or removed in a stepwise manner as the structure converged, until all interproton separations (Table VIII) were satisfactorily accommodated. The inclusion of further distance restraints, particularly those involving Thy H1′ and BH2(2′) protons, required that certain corresponding bases on each strand of the DNA effectively became nonequivalent and degeneracy was thus lost (e.g., A5 ≠ A17, A6 ≠ A18).

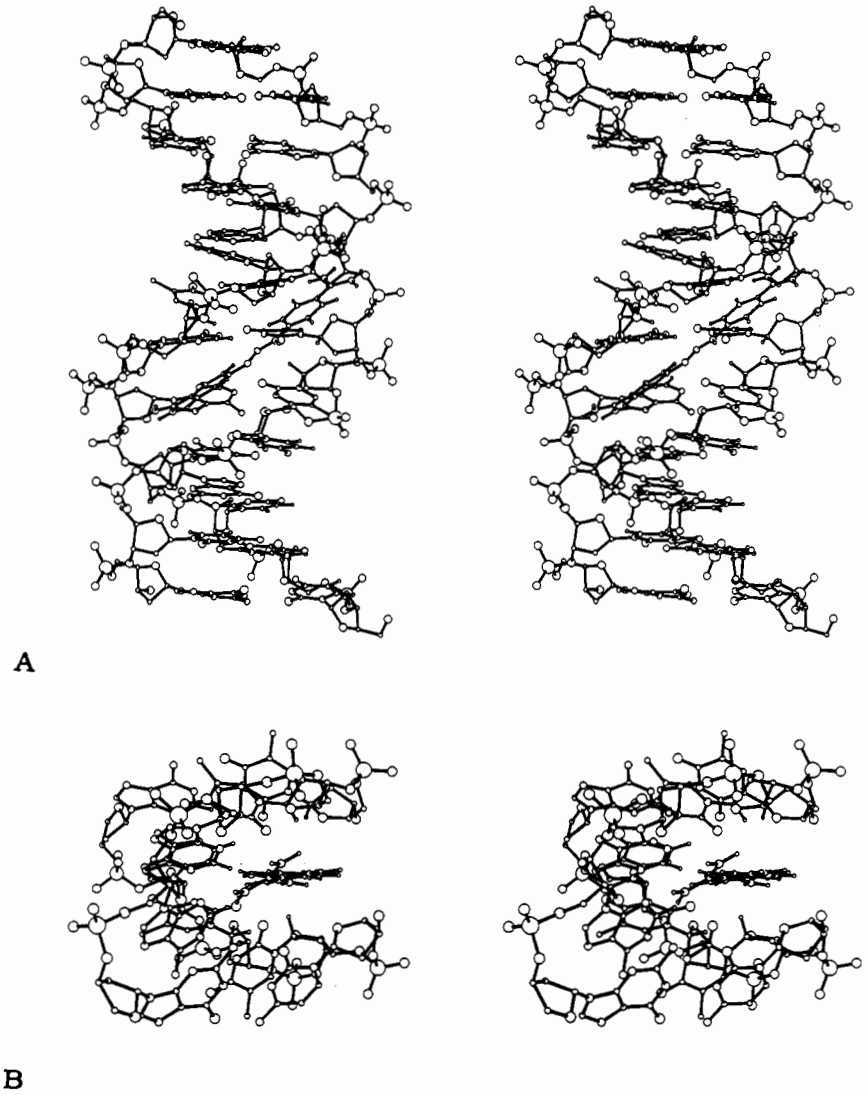

FIGURE 10: Stereoviews of the refined *Eco*RI–berenil complex generated by using PLUTO. (A, Top) View of the entire complex looking into the minor groove (H atoms other than those used in the refinement have been removed for clarity). (B, Bottom) Close-up view of the minor groove looking from the 3′-end (5′-AATTC-3′) showing planarity of the ligand and its alignment with the groove walls (all H atoms are included).

As the refinement converged, it was apparent that the berenil molecule is uniquely located at a focus that spans the A6pT7pT8 site on strand 1 and necessarily involves NOE contacts with the nucleotides on the A17pA18pT19 base sequence on the complementary strand. A total of 19 interproton distance restraints and 24 glycosidic dihedral constraints were used to generate the ultimate structures, for which rms gradients of <0.06 kJ mol^{-1} nm^{-1} were achieved. NOE violations were <±0.02 nm prior to final conjugate-gradient relaxation and <±0.06 nm in the fully refined models.

Examination of the structures associated with the berenil in each of its two possible orienttions showed that the binding is more exothermic by ≈40 kJ mol^{-1} when the triazene core is aligned as NH—N=N rather than N=N—NH with respect to the 5′-A6pT7pT8 binding site. This alignment is favored largely due to the lower induced perturbation of the DNA ($\Delta\Delta H_{pert} \approx 34$ kJ mol^{-1}) by the ligand, rather than by specific van der Waals or electrostatic nonbonded energy terms in the complex. A similar orientation effect has recently been predicted for the interaction of berenil with the *Tyr* T DNA sequence (Laughton et al., 1990).

Figure 10 shows the final structure of the *Eco*RI–berenil complex; the NOE assignments and degeneracies employed are listed in Table VIII. The ligand is asymmetrically located with respect to the diad axis of the duplex and is unambiguously bound to the minor groove of the oligonucleotide at the 5′-ATT-3′ site. This sequence is equivalent by symmetry to the 5′-AAT-3′ binding site revealed by X-ray crystallography for the same complex (Brown et al., 1990). Further, the berenil molecule spans three base pairs (bp), in accord with the estimate of binding-site size from both DNase I and hydroxyl radical footprinting studies (Portugal & Waring, 1987; Laughton et al., 1990) and the crystal structure (Brown et al., 1990). This observation refutes the conclusions from earlier modeling studies that berenil binds to DNA via adjacent or 1,2-bp models (Gresh & Pullman, 1984; Pearl et al., 1987; Gago et al., 1989). The nonadjacent or 1,3-bp site revealed in this study is, however, in accord with the preferred low-energy "class 2" binding sites predicted from more extended molecular mechanics studies with this ligand (Brown et al., 1990; Laughton, 1990; Jenkins and Neidle, unpublished data).

The berenil molecule is closely isohelical with the floor of the DNA minor groove (Figure 10B), and the phenyl residues of the ligand lie parallel to the hydrophobic walls. Induced torsional rotations are concerted and confined to <8°; however, the amidinium group at the 3′-end of the site is significantly rotated (25°) from the plane of the aromatic ring. General planarity is retained and there is minimal DNA-induced

twisting or bending. Further, the central triazene nitrogen atom lies in the mean plane defined by the Thy 7/Ado 18 base pair.

The terminal amidinium groups of the ligand are in close contact with the bases Ado 6 and Ado 17, with (Ado)N3···H(amidine) hydrogen-bonded separations of 0.218 and 0.248 nm, respectively. Further, the amidinium moiety at the 3′-end of the site forms weaker hydrogen bonds with the exocyclic N2 atom of Gua 16, where the N2···N(amidine) distance is 0.277 nm, and the O4′ deoxyribose ring atoms of Ado 17 and Ado 18, where the O4′···N(amidine) separations are 0.337 and 0.317 nm, respectively. The binding site revealed in aqueous solution closely resembles that shown by X-ray crystallography (Brown et al., 1990) but differs in that the ligand is more central with respect to the diad axis of the DNA; the translation is 0.5 base pair. The crystal structure has shown that a bridging water molecule mediates between the adenine N3 atom and the amidinium group of the bound berenil at the 3′-end of the 5′-ATT-3′ binding site. The present study, however, suggests that in solution this hydrogen bonding may be direct, since low-energy models can be generated that satisfy the observed NOEs. It should be noted that solvent and solvation effects were not included in the refinements. No attempt was made to refine structures with water-mediated or -bridged hydrogen-bond arrangements. The ligand displacement revealed by NMR confirms earlier calculations (Brown et al., 1990) that the enthalpic energy well for complexation is likely to be broad for the spanned d(·AATT·) sequence, with competitor binding sites separated by only ca. 4 kJ mol^{-1}.

The dodecamer in the *Eco*RI complex adopts a general B-type DNA conformation with little disruption to the parallel stacking of (Ado)N3···H(amidine) base pairs. Ligand-induced perturbations, manifest primarily as increased roll and tilt angles for the Thy 8/Ado 17 and Cyt 9/Gua 16 base pairs (Figure 10A), are generally confined to the ATT(C) site and do not propagate significantly beyond this sequence. However, we note that the distortions induced at the 3′-end of the binding site are sensitive to the parameterization used for the ligand, particularly torsional factors associated with the charged amidine groups. Further, there was no evidence for either undue base roll or tilt in the absence of berenil. The localized DNA conformational changes that result from the binding of berenil are, however, broadly in accord with induced chemical shift changes for the major-groove resonances in this region (cf. Figure 6). Helix analysis of the complex shows an average helical rise of 0.31 ± 0.07 nm and a mean helical twist of 39 ± 9° (9.2 base pairs per turn), compared with 37 ± 5° for the free dodecamer (9.7 base pairs per turn). This indicates that the conformation of the DNA is not significantly altered by the minor groove binding molecule.

After submission of our manuscript, a paper appeared by Yoshida et al. (1990) on an NMR study of a 1:1 complex of berenil with $d(GCAATTGC)_2$. They concluded that the ligand binds in the minor groove in the AATT segment. Preliminary modeling suggested that berenil binds by hydrogen bonding of its amidinium protons to the N3 of adenines. This is in broad agreement with our findings obtained with the longer DNA sequence.

ACKNOWLEDGMENTS

We thank Dr. S. Martin for recording the CD spectra and Dr. J. Feeney for critical appraisal of the manuscript.

REFERENCES

Arnott, S., Chandrasekaran, R., Hall, I., & Puigjaner, L. C. (1983) *Nucleic Acids Res. 11*, 4141–4155.

Baker, B. R., & Erickson, E. H. (1967) *J. Med. Chem. 10*, 1123–1128.

Bax, A., & Davis, D. G. (1985) *J. Magn. Reson. 65*, 355–360.

Bax, A., & Lerner, L. (1988) *J. Magn. Reson. 79*, 429–438.

Brodersen, R., Loewe, H., & Ott, H. (1958) U.S. Patent 2,838,485.

Brooks, B. R., Bruccoleri, R. E., Olafson, B. D., States, D. J., Swaminathan, S., & Karplus, M. (1983) *J. Comput. Chem. 4*, 187–217.

Brown, D. G., Sanderson, M. R., Skelly, J. V., Jenkins, T. C., Brown, T., Garman, E., Stuart, D. I., & Neidle, S. (1990) *EMBO J. 9*, 1329–1334.

Brünger, A. T. (1988) *X-PLOR Manual*, version 1.5, Yale University.

Brünger, A. T. (1990) in *Molecular Dynamics: Applications in Molecular Biology* (Goodfellow, J. M., Ed.) pp 137–178, Macmillan Press, London.

Chary, K. V., Hosur, R. V., Govil, G., Chen, C.-q., & Miles, H. T. (1988) *Biochemistry 27*, 3858–3867.

De Clercq, E., & Dann, O. (1980) *J. Med. Chem. 23*, 787–795.

Dickerson, R. E., & Drew, H. R. (1981) *J. Mol. Biol. 149*, 761–786.

Dieckmann, S. (1989) *EMBO J. 8*, 1–4.

Forster, M. J. (1989) *J. Magn. Reson. 84*, 580–584.

Forster, M. J., & Lane, A. N. (1990) *Eur. Biophys. J. 18*, 347–355.

Fratini, A. V., Kopka, M. L., Drew, H. R., & Dickerson, R. E. (1982) *J. Biol. Chem. 257*, 14686–14707.

Gago, F., Reynolds, C. A., & Richards, W. G. (1989) *Mol. Pharm. 35*, 232–241.

Gao, X., & Patel, D. J. (1989) *Q. Rev. Biophys. 22*, 93–138.

Gorenstein, D. G., Schroeder, S. A., Fu, J. M., Metz, J. T., Roongta, V., & Jones, C. R. (1988) *Biochemistry 27*, 7223–7237.

Gresh, N., & Pullman, B. (1984) *Mol. Pharmacol. 25*, 452–455.

Gronenborn, A. M., & Clore, G. M. (1989) *Biochemistry 28*, 5978–5984.

Gupta, R. K., Ferretti, J. A., Becker, E. D., & Weiss, G. H. (1980) *J. Magn. Reson. 38*, 447–452.

Hare, D. R., Wemmer, D. E., Chou, S.-H., Drobny, G., & Reid, B. R. (1983) *J. Mol. Biol. 171*, 319–336.

Hore, P. J. (1983) *J. Magn. Reson. 55*, 283–300.

Kim, R., Modrich, P., & Kim, S.-H. (1984) *Nucleic Acids Res. 12*, 7285–7292.

Lane, A. N. (1989) *Biochem. J. 259*, 715–724.

Lane, A. N. (1990) *Biochim. Biophys. Acta 1049*, 189–204.

Lane, A. N., & Forster, M. J. (1989) *Eur. Biophys. J. 17*, 221–232.

Lane, A. N., Lefèvre, J.-F., & Jardetzky, O. (1986) *J. Magn. Reson. 66*, 201–218.

Laughton, C. A., Jenkins, T. C., Fox, K. R., & Neidle, S. (1990) *Nucleic Acids Res. 18*, 4479–4488.

Lefèvre, J.-F., Lane, A. N., & Jardetzky, O. (1987) *Biochemistry 26*, 5076–5089.

Lefèvre, J.-F., Lane, A. N., & Jardetzky, O. (1988) *Biochemistry 27*, 1086–1094.

Marion, D., & Wüthrich, K. (1983) *Biochem. Biophys. Res. Commun. 124*, 774–783.

McClarin, J. A., Frederick, C. A., Wang, B.-C., Greene, P. G., Boyer, H. W., Grable, J., & Rosenberg, J. M. (1986) *Science 234*, 1526–1541.

Mirau, P. (1988) *J. Magn. Reson. 80*, 439-447.
Neidle, S., Pearl, L. H., & Skelly, J. V. (1987) *Biochem. J. 243*, 1-13.
Nerdal, W., Hare, D. R., & Reid, B. R. (1989) *Biochemistry 28*, 10008-10021.
Nilsson, L., & Karplus, M. (1986) *J. Comput. Chem. 7*, 691-716.
Nilsson, L., Clore, G. M., Gronenborn, A. M., Brünger, A. T., & Karplus, M. (1986) *J. Mol. Biol. 188*, 455-475.
Orozco, M., Laughton, C. A., Herzyk, P., & Neidle, S. (1990) *J. Biomol. Struct. Dyn. 8*, 359-373.
Ott, J., & Eckstein, F. (1985) *Biochemistry 24*, 2530-2535.
Patel, D. J., Kozlowski, S. A., Marky, L. A., Broka, C., Rice, J. A., Itakura, K., & Breslauer, K. J. (1982) *Biochemistry 21*, 428-436.
Patel, D. J., Ikuta, S., Kozlowski, S., & Itakura, K. (1983) *Proc. Natl. Acad. Sci. U.S.A. 80*, 2184-2188.
Pearl, L. H., Skelly, J. V., Hudson, B. D., & Neidle, S. (1987) *Nucleic Acids Res. 15*, 3469-3478.
Portugal, J., & Waring, M. J. (1987) *Eur. J. Biochem. 167*, 281-289.
Reid, B. R., Banks, K., Flynn, P., & Nerdal, W. (1989) *Biochemistry 28*, 10001-10007.
Rinkel, L. J., & Altona, C. (1987) *J. Biomol. Struct. Dyn. 4*, 621-649.
Rinkel, L. J., van der Marel, G. A., van Boom, J. H., & Altona, C. (1987) *Eur. J. Biochem. 186*, 87-101.
Saenger, W. (1984) *Principles of Nucleic Acid Structure*, Springer-Verlag, Berlin.
Tidor, B., Irikura, K., Brooks, B. R., & Karplus, M. (1983) *J. Biomol. Struct. Dyn. 1*, 231-252.
van de Ven, F. J. M., & Hilbers, C. W. (1988) *Eur. J. Biochem. 178*, 1-38.
Wagner, G., & Wüthrich, K. (1979) *J. Magn. Reson. 33*, 675-680.
Walton, A. R., Jenkins, T. C., & Neidle, S. (1990) *Acta Crystallogr.* (in press).
Williamson, J. R., & Boxer, S. G. (1989) *Biochemistry 28*, 2819-2831.
Woessner, D. E. (1962) *J. Chem. Phys. 37*, 647-654.
Yoshida, M., Banville, D. L., & Shafer, R. H. (1990) *Biochemistry 29*, 6585-6592.
Zimmer, C., & Wähnert, U. (1986) *Prog. Biophys. Mol. Biol. 47*, 31-112.

Kinetic Analysis of Protein Kinase C: Product and Dead-End Inhibition Studies Using ADP, Poly(L-lysine), Nonhydrolyzable ATP Analogues, and Diadenosine Oligophosphates†

Phillip S. Leventhal and Paul J. Bertics*
Department of Physiological Chemistry, University of Wisconsin—Madison, Madison, Wisconsin 53706
Received July 17, 1990; Revised Manuscript Received October 15, 1990

ABSTRACT: The kinetic mechanism of protein kinase C (PKC) was analyzed via inhibition studies using the product MgADP, the nonhydrolyzable ATP analogue adenosine 5′-(β,γ-imidotriphosphate) (MgAMPPNP), the peptide antagonist poly(L-lysine), and several naturally occurring ATP analogues that are produced in rapidly growing cells, i.e., the diadenosine oligophosphates (general structure: Ap_nA; n = 2-5). By use of histone as the phosphate acceptor, the inhibition of PKC by MgAMPPNP and MgADP was found to be competitive vs MgATP (suggesting that these compounds bind to the same enzyme form), whereas their inhibition vs histone was observed to be noncompetitive. In contrast, the inhibition by poly(L-lysine) appeared competitive vs histone but uncompetitive vs MgATP, which is consistent with a model wherein MgATP binding promotes the binding of poly(L-lysine) or histone. With the diadenosine oligophosphates, the degree of PKC inhibition was found to increase according to the number of intervening phosphates. The diadenosine oligophosphates Ap_4A and Ap_5A were the most effective antagonists of PKC, with Ap_5A being approximately as potent as MgADP and MgAMPPNP. However, as opposed to MgADP and MgAMPPNP, Ap_4A and Ap_5A appear to act as noncompetitive inhibitors vs both MgATP and histone, suggesting that they can interact at several points in the reaction pathway. These studies support the concept of a steady-state mechanism where MgATP binding preferentially precedes that of histone, followed by the release of phosphorylated substrate and MgADP. Furthermore, these results indicate a differential interaction of the diadenosine oligophosphates with PKC, when compared to other adenosine nucleotides.

Protein kinase C (PKC) consists of a family of homologous calcium- and phospholipid-dependent enzymes that have been extensively characterized with respect to their role in cellular regulation (Nishizuka, 1986, 1988). PKC has been implicated in mediating hormone signal transduction, in modulating gene expression, and in controlling cellular growth and differentiation (Nishizuka, 1986, 1988). Because of the importance of PKC in these processes, many investigations have focused on its structure (Coussens et al., 1986; Knopf et al., 1986; Makowske et al., 1986; Housey et al., 1987; Ohno et al., 1987; Ono et al., 1988), as well as its regulation and physical properties (Nishizuka, 1986, 1988; Bazzi & Nelsestuen, 1987; Huang et al., 1988; Leach et al., 1988; Kaibuchi et al., 1989; Lowndes et al., 1990; Hannun & Bell, 1990).

In general, PKC phosphorylates substrates on serine/threonine residues located near basic amino acids, a process that usually requires calcium and phospholipid (Turner et al.,

† This work was supported by grants to P.J.B. from the Life and Health Insurance Medical Research Fund and from the Shaw Scholar Program of the Milwaukee Foundation.
* Address correspondence to this author.

0006-2960/91/0430-1385$02.50/0